HAL
open science

Electron energy-loss magnetic chiral dichroism of magnetic iron film affected by an underlayer in a double-layer structure

X. Fu, K. Wu, V. Serin, Bénédicte Warot-Fonrose, Q. He, R. Yang, L. Zhang, X. Huang

To cite this version:

X. Fu, K. Wu, V. Serin, Bénédicte Warot-Fonrose, Q. He, et al.. Electron energy-loss magnetic chiral dichroism of magnetic iron film affected by an underlayer in a double-layer structure. Applied Physics Letters, 2019, 115 (11), pp.112401. 10.1063/1.5100245 . hal-02349164

HAL Id: hal-02349164

https://hal.science/hal-02349164

Submitted on 6 Nov 2020

HAL is a multi-disciplinary open access archive for the deposit and dissemination of scientific research documents, whether they are published or not. The documents may come from teaching and research institutions in France or abroad, or from public or private research centers.

L'archive ouverte pluridisciplinaire **HAL**, est destinée au dépôt et à la diffusion de documents scientifiques de niveau recherche, publiés ou non, émanant des établissements d'enseignement et de recherche français ou étrangers, des laboratoires publics ou privés.

Applied Physics Letters ARTICLE scitation.org/journal/apl

Electron energy-loss magnetic chiral dichroism of magnetic iron film affected by an underlayer in a double-layer structure

Cite as: Appl. Phys. Lett. **115**, 112401 (2019); doi: 10.1063/1.5100245
Submitted: 16 April 2019 · Accepted: 26 August 2019 ·
Published Online: 9 September 2019

View Online Export Citation CrossMark

X. Fu,[1,a)] K. Wu,[1] V. Serin,[2] B. Warot-Fonrose,[2] Q. He,[1] R. Yang,[1] L. Zhang,[1] and X. Huang[1]

AFFILIATIONS

[1]College of Materials Science and Engineering, Chongqing University, Chongqing, 400044, China
[2]Univ Toulouse, CEMES-CNRS UPR 8011, F-31055 Toulouse, France

[a)]xiaoxiao.fu@outlook.com

ABSTRACT

The electron energy-loss magnetic chiral dichroism (EMCD) technique has been generally applied to single-phase magnetic crystals while rarely used for composite structures. It is mainly due to the lack of in-depth understanding of EMCD in the latter case where an additional phase may present under or above the investigated magnetic phase in the electron beam path. Here, we report EMCD signals acquired on a 15-nm-thick magnetic iron film with different thicknesses of the MgO substrate underlayer. By comparison, for areas with total thicknesses of $t = 0.59\lambda$ and $t = 1.02\lambda$ expressed with the mean free inelastic path of electron λ, the relative dichroic signals at the Fe-L_3 edge are 3.8%±1.0% and 3.5%±1.6%, respectively, demonstrating no significant difference within the error range. However, the dichroic signal intensity at the Fe-L_2 edge peak is 77.6% larger in the thinner area of $t = 0.59\lambda$. Accordingly, the extracted m_L/m_s ratio of Fe 3d moments is 63% smaller in the thinner area even after the plural scattering is removed. Then, we confirm that the presence of an additional nonmagnetic phase under a magnetic iron crystal can noticeably affect the quantified value of the m_L/m_s ratio of iron moment determined from the EMCD measurements. Furthermore, the larger thickness of the underlayer may result in relatively higher valuation of the m_L/m_s ratio of the upper layer. A correction method, considering the different influence of the underlayer on the Fe-L_3 and L_2 edges, is in demand for developing potential applications of the EMCD technique to such composite nanomaterial systems.

Published under license by AIP Publishing. https://doi.org/10.1063/1.5100245

Electron energy-loss magnetic chiral dichroism (EMCD) is an electron energy-loss spectroscopy (EELS)-based technique to locally characterize element-specific spin and orbital magnetic moments in crystalline materials.[1–3] The magnetic information is obtained from the EELS spectra recorded at two different positions on the diffraction plane, where different combinations of electron scattering vectors give rise to left- and right-handed polarized virtual photons in analogy with circular polarized X-rays in the synchrotron-based X-ray magnetic circular dichroism (XMCD) technique.[1] Since EMCD was first demonstrated by Schattschneider *et al.*,[1] much effort has been made to develop it into a routine magnetic characterization technique in the transmission electron microscope (TEM).[4–14] Various EMCD experimental setups, for instance the energy spectrum imaging,[4,5] double aperture $q - E$ mode,[6] spatially resolved EELS mode,[7] and scanning TEM,[8,9] have been proposed to improve the signal to noise ratio and the spatial resolution. In addition, the signal interpretation regarding the magnetic moment quantification has been widely concerned. The EMCD signal is not only simply affected by the intrinsic magnetism but also modulated by the dynamic electron diffraction condition which is related to the crystal structure, crystal orientation, and specimen thickness.[3,10,11] With a deep understanding of the dynamic diffraction, the quantification of element-specific and even site-specific orbital and spin moments has been experimentally realized.[11,12] Moreover, the theoretical simulation of the relative EMCD signal in various diffraction conditions has been widely applied for optimizing the experimental conditions[13,14] of EMCD or broadening its applications.[15]

For the moment, the interpretation of quantitative results extracted from the EMCD signal is essentially based on an assumption that only one single-phase crystal is present in the electron beam path for each acquisition. Some EMCD experiments in the literature are actually in accordance with the assumed condition. For instance, experiments were performed on a single crystal in polycrystalline materials of Fe,[9] Co,[16] Ni,[16] or their oxides[7,17] or on epitaxially grown thin layers of single-crystalline Fe, Mn, and their compounds observed from

Published under license by AIP Publishing

the cross-sectional view.[10,14,18,19] However, the assumption may fail if the EMCD technique is applied to other widely used systems such as core-shell structures, embedded nanoparticles, and multilayers observed along the out-of-plane direction. More than one material may present in the beam direction, considering that a complete removal of one component material in these composite structures may be difficult or possibly introduces changes in magnetic moments of other components. Accordingly, there will be many open questions, for instance, how to understand the dynamic electron diffraction effects in such systems and how under the crystal the upper one affects the EMCD signal of each other. Actually, there have been reports of EMCD signals acquired on similar models, i.e., plane-view TEM samples of Fe thin films with GaAs[1] and MgO[5,6] substrates, while there is little discussion about the influence of substrate underlayers on the dichroic signal of the Fe film.

In this letter, we performed EMCD experiments on a plane-view sample of a single-crystalline iron thin film on MgO(001) substrates. EMCD signals of Fe-$L_{2,3}$ edges were acquired at two different areas where the electron beam passed through the same thickness of the iron layer but a different thickness of the MgO underlayer. Comparisons were made on the EMCD signals and the corresponding orbital to spin moment ratios of Fe 3d moment between the two areas. The influence of the MgO underlayer on the EMCD of the magnetic iron layer was discussed.

An iron thin film was deposited on a MgO (001) single crystal substrate via pulsed-laser deposition. Cross-sectional and plane-view TEM specimens were prepared with conventional methods including mechanical thinning (Multipre^{TM} system) and Ar^+ ion-beam milling (PIPS-Gatan). The plane-view one, for instance, was first polished from the MgO substrate side until 10 μm and then milled from the same side to achieve electron transparency. TEM experiments were performed at room temperature on a Tecnai F20 microscope operating at 200 kV fitted with a postcolumn energy filter (Gatan GIF Quantum). The thickness uniformity and crystal structure of the iron layer were checked by bright field and high resolution TEM in the cross-sectional sample. EELS and EMCD experiments were performed on the plane-view sample. It should be noted that the plane-view sample was intentionally installed on the TEM holder in a way that the electron beam can first pass through the iron layer and then MgO under it. The ferromagnetic iron layer of the plane-view sample was constantly magnetized out-of-plane, in the direction parallel to the electron beam, to saturation by a magnetic field of 2 T from the objective lens in TEM (see the magnetic hysteresis curves in Fig. S1 in the supplementary material).

For EMCD experiments, a nearly parallel beam with a probe size of around 200 nm in diameter was used to illuminate the sample. Diffraction patterns were obtained in the conventional selected area electron diffraction (SAED) geometry. A $\pm(110)$ three-beam diffraction condition was achieved by tilting the Fe crystal by 5 degrees from the [001] zone axis. Two chiral positions, the symmetrical points on the Thales circle passing through the transmission and Fe(110) Bragg spots, were successively selected by the objective aperture. Accordingly, two EELS signals at Fe-$L_{2,3}$ edges included in the energy range from 650 eV to 854 eV were recorded, and normalization of the two signals was performed by aligning the integrate values under them in the range from 760 eV to 800 eV. Orbital to spin moment ratios of iron along the electron beam axis were extracted from EMCD signals, which are the difference of the two EELS signals, with EMCD Sum Rules[3] using Matlab. Statistical results were obtained by repeatedly acquiring EMCD signals at the same experimental condition. More detailed information about the principle and experimental setups of EMCD are presented in Fig. S2 in the supplementary material. Meanwhile, low-loss EELS spectra were also acquired without any objective aperture, for checking the relative thickness t/λ of the observed area and the plasmon scattering, where t is the local thickness and λ is the mean free inelastic path of the electron. The same experimental process was applied to two different areas, and their experimental results were compared with each other and also with the theoretical result simulated with a program demonstrated in Ref. 20. This program, on the basis of the simulation of elastic and inelastic electron scattering, can be used to simulate the dependence of the relative EMCD signal of the single-crystalline sample on various experimental parameters such as sample tilt and sample thickness.[20]

Figure 1(a) presents a bright field TEM image of the cross section Fe/MgO(001) sample observed from the MgO [010] zone axis. The thickness of the iron layer is quite uniform, which is measured to be 15 nm. The SAED pattern of the area in the dashed circle of Fig. 1(a) is presented in Fig. 1(b), indicating that the iron layer is single crystalline and its epitaxial relationship with the MgO substrate is Fe[110](001)//MgO[100](001). A high resolution TEM image of the Fe/MgO interface in Fig. 1(c) verifies that the iron layer was well epitaxially grown on the substrate. In this image, only Fe(110) lattice planes are resolved for the iron layer and both MgO(002) and (200) planes are resolved for the substrate. The Fe(110) interplanar spacing is measured to be

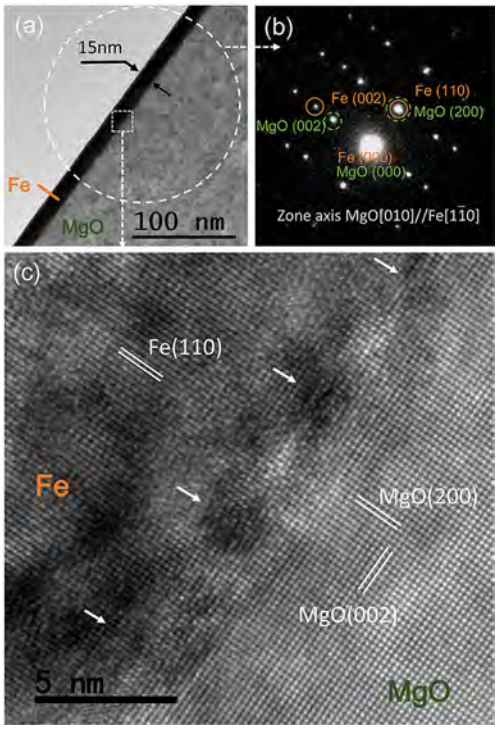

FIG. 1. (a) A bright field TEM image of the cross-sectional iron thin film on the MgO(001) substrate along the MgO[010]//Fe[1$\bar{1}$0] zone axis. (b) The diffraction pattern of the area in the dashed circle in (a). (c) The high resolution TEM image of the area in the dotted square in (a).

Published under license by AIP Publishing

$d_{Fe(110)} = 0.2028$ nm,[21] about 4% smaller than the MgO(002) interplanar spacing of $d_{MgO(200)} = 0.2110$ nm.[22] The tensile stress of MgO on the Fe lattices has been released at the interface through the lattice mismatch dislocations, which introduce the contrasts indicated by white arrows in Fig. 1(c). Additionally, there is interdiffusion of Fe atoms into the MgO substrate, in the variation of ∼3.5% along the interface. More information on the interface can be seen in Fig. S3 in the supplementary material.

Figure 2 demonstrates the experimental results of electron diffraction and low-loss EELS on the plane-view sample of Fe/MgO(001). Figure 2(a) shows a conventional low-magnification TEM image. The areas of about 200 nm in diameter in the two circles marked as A and B are selected to be observed. Area A is closer to the vacuum area than area B. The curvilinear contrasts that are most obvious near the vacuum are bend contours, and the areas in A and B are considered as flat without bending. Figure 2(b) compares the low-loss EELS spectra acquired at the two areas. Their zero-loss peak intensities have been normalized to 1 and centered at 0 eV. Both spectra show plasmon peaks approximately at the energy loss of 22 eV with the full width at half maximum above 18 eV, while the peak height for area B is 45% larger than that for area A. Determined with a log-ratio method[23] from the low-loss spectra intensity, the thickness $t = 1.02\lambda$ of area B is larger than $t = 0.59\lambda$ of area A. The absolute values of the thickness in areas A and B are estimated to be around 60 nm and 100 nm. Figs. 2(c) and 2(d) show the corresponding diffraction patterns acquired at areas A and B along the zone axis of Fe[001]//MgO[001]. It can be seen that two sets of diffraction spots are resolved in both Figs. 2(c) and 2(d).

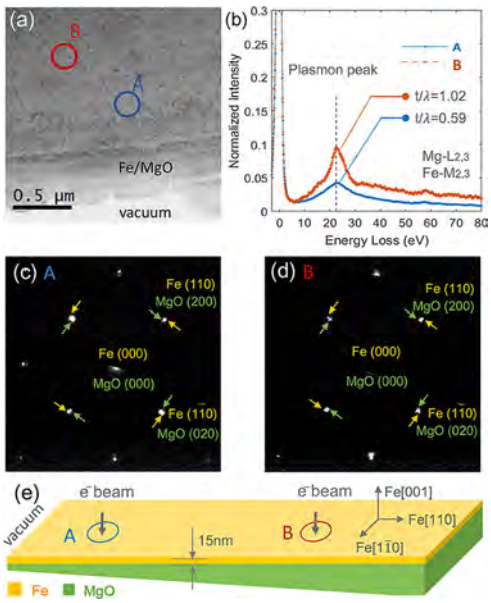

FIG. 2. (a) A conventional low-magnification TEM image of the Fe/MgO(001) plane-view sample, in which area A and area B are marked with blue and red circles, respectively. (b) The low-loss EELS spectra of area A and area B with the zero-loss peak normalized to 1 and centered at 0 eV; the diffraction pattern acquired in (c) area A and (d) area B along the MgO(001)//Fe(001) zone axis and the yellow and green arrows indicate the diffraction spots of Fe and MgO, respectively. (e) A sketch to demonstrate the difference of areas A and B in the relative thickness of Fe and MgO crystals along the electron beam.

We index the patterns and ensure that one set of spots marked by yellow arrows are from the body-centered cubic (bcc) Fe crystal, and the other ones marked by green arrows are from face-centered cubic (fcc) MgO. The distances from spot Fe(110) and MgO(200) to the transmission spot **0** have a ∼4% difference, so as the distance from Fe(1$\bar{1}$0) and MgO(002). It agrees with the difference of $d_{Fe(110)}$ and $d_{MgO(200)}$ interplanar spacings mentioned above. Thus, we ensure that areas A and B are double-layer structures of Fe and MgO, and the Fe lattice is relaxed on MgO. Now, we can say that there is a 15-nm-thick single-crystalline bcc Fe thin film with single-crystalline fcc MgO underlayers presenting in the electron beam path in both areas A and B, and the MgO layer is relatively thinner in area A, as sketched in Fig. 2(e).

Before demonstrating the experimental EMCD results of the two areas, Fig. 3(b) shows the simulated thickness-dependent relative dichroic signal for a bcc Fe crystal orientated in a ±(110) three-beam

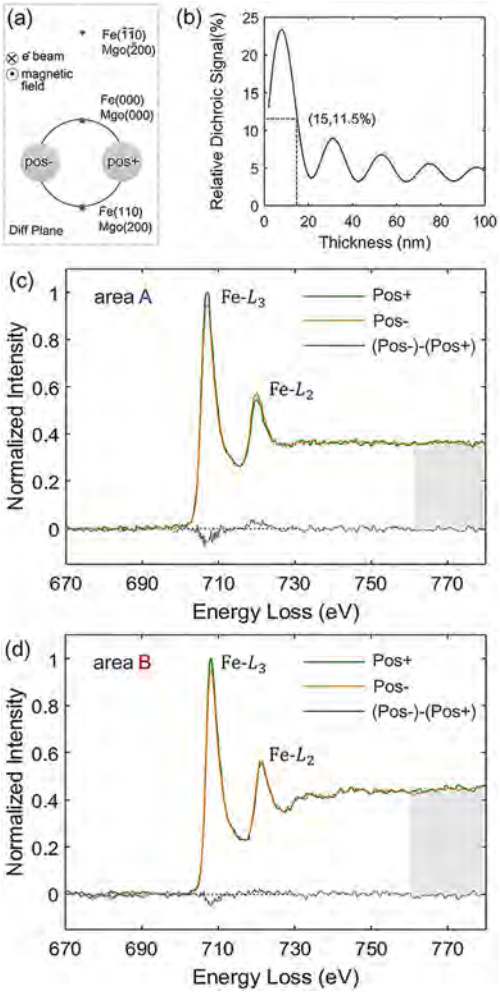

FIG. 3. (a) A sketch of the chiral positions in the diffraction plane. (b) The simulated relative dichroic signal of Fe-L_3 changing with the thickness of Fe in the ±(110) three-beam condition; the typical EELS and EMCD spectra (before the plural scattering removed) measured in (c) area A and (d) area B, and the shadow areas indicate the normalization region.

Published under license by AIP Publishing

condition as shown in Fig. 3(a). The relative dichroic signal here is defined as the difference divided by the sum of the two chiral EELS spectra. We can see that the relative signal intensity fluctuates with the thickness of the Fe crystal due to dynamic electron diffraction effects, and the intensity is as high as 11.5% at the thickness of 15 nm which is the thickness of our magnetic iron film. It should be noted that the thickness in Fig. 3(b) does not include the thickness of other crystals as underlayers but only for the magnetic iron layer.

Typical experimental EELS and EMCD signals at Fe-$L_{2,3}$ edges of areas A and B are shown in Figs. 3(c) and 3(d). It can be seen in both (c) and (d) that the two EELS spectra acquired at chiral positions show an intensity difference at the Fe-L_3 and Fe-L_2 edges, and the EMCD signals have opposite signs at the two edges. The noise level of the EMCD spectra, defined by the standard deviation of the EMCD signal in the pre-edge energy range divided by the average intensity of two EELS spectra at the Fe-L_3 peak, is 0.6% for area A and 1.0% for B. The relative dichroic signal intensity at the Fe-L_3 edge is measured to be 3.8% $\pm$ 1.0% for area A and 3.5% $\pm$ 1.6% for area B. The error bar is determined from several EMCD spectra repeatedly acquired at the same area in the same experiment condition. Both experimental values are smaller than the theoretical value of 11.5%. Actually, this discrepancy in similar material systems is generally presented in the literature. For instance, in Ref. 1, the value for a 10-nm-thick Fe thin film on the GaAs substrate of unknown thickness is measured to be 3.5% (following our definition of the relative dichroic signal), smaller than its theoretical value of 16.1%. Another experimental value is about 3.7% in Ref. 5 for a 10-nm-thick Fe thin film on the MgO substrate of unknown thickness in a similar $\pm(110)$ three-beam condition as in our experiment. The information of the substrate thickness is not provided and discussed in these references. There are several possible causes of the relatively small experimental dichroic signal. First, the integration of the signal over the finite spectrometer entrance aperture and the nonzero convergence angle reduces the dichroic effect.[1] Second, the electron beam passed through two phases which are bcc Fe and fcc GaAs or MgO. Their interface with imperfect dislocations and the difference in their lattice parameters make the real dynamic diffraction condition much different from the ideal condition assumed in the simulation and thus change the relative dichroic signal.

When comparing the two experimental values, no significant difference of the relative dichroic signal at the Fe-L_3 edge for areas A and B is observed, given a 0.4% difference in their noise levels of EMCD signals and 0.6% difference in their error ranges. However, the EMCD signal intensity at the Fe-L_2 edge peak is 77.6% lower for area B. Accordingly, the m_L/m_s ratio of Fe 3d moment calculated from the EMCD signals with EMCD sum rules is determined to be 0.11 ± 0.02 for area A with $t = 0.59\lambda$ and 0.24 ± 0.03 for area B with $t = 1.02\lambda$. The m_L/m_s value for area B is 118% larger than the value for area A, and both values are larger than 0.09 which is measured from a similar bcc iron layer with a thickness of $t = 0.23\lambda$ without the presence of the MgO substrate in Ref. 24. One cause of the discrepancy between the values for areas A and B may be the difference in plural scattering. In Figs. 3(c) and 3(d), we can easily see that the EELS spectra after the Fe-L_2 edge have higher intensity for area B and especially the peak at the energy of around 730 eV which is in accordance with the plasmon peak at 22 eV. Actually, the plasmon scattering has influence on the dichroic signal.[24] For instance, it has been derived in Ref. 24 that the plural scattering has little influence on the dichroic signal intensity at the Fe-L_3 edge but noticeably decreases the one at the Fe-L_2 edge for bcc Fe, thus increasing the measured m_L/m_s ratio of Fe 3d moment. After removing the plasmon scattering by deconvoluting EELS spectra in Figs. 3(c) and 3(d) by low-loss EELS spectra in Fig. 2(b), the m_L/m_s ratio is 0.08 ± 0.02 for area A with $t = 0.59\lambda$ and 0.13 ± 0.03 for area B with $t = 1.02\lambda$. The m_L/m_s value for area B is still 63% larger than the value for area A. Given the same thickness of the magnetic iron layer with saturated magnetization for the two areas, we confirm that the presence and the thickness variation of the MgO underlayer have a significant influence on the dichroic signal of the iron film and the extracted m_L/m_s ratio of Fe 3d moment. A larger underlayer thickness may results in higher valuation of the m_L/m_s ratio. The results are contrary to the common understanding of the known EMCD sum rules, in which the dynamic diffraction effects and the intrinsic magnetism are two independent factors to influence the dichroic signal intensity, and the value of m_L/m_s does not change with any variation of diffraction conditions. As to the cause of the contradictory, the possibility of different intrinsic magnetism for the two areas has been carefully ruled out by our previous discussion, and the dynamic electron diffractions for the case of double layers in the electron beam path should be concerned. It is possibly due to that the different influences of the dynamic diffractions in MgO underlayers of different thicknesses and the influence of the imperfect Fe/MgO interface on the intensity of Fe-L_3 and L_2 edges have not been taken into consideration in the known sum rules. An investigation of a relative correction method is in demand.

In summary, we investigated the EMCD signal of a 15-nm-thick magnetic iron film with a MgO substrate underlayer in the electron beam path. Two areas, $t = 0.59\lambda$ and $t = 1.02\lambda$ respectively, with the same thickness of iron but different thicknesses of MgO were selected and carefully checked with electron diffraction and low-loss EELS. The relative dichroic signals at the Fe-L_3 edge for the two selected areas present no significant difference within the error range, while they are more than three times smaller than the theoretical value that is simulated on a single-crystalline 15-nm-thick iron layer. In addition, the dichroic signal at the Fe-L_2 edge relative to the Fe-L_3 edge is smaller for the area of $t = 1.02\lambda$ with a thicker MgO underlayer, and, correspondingly, the measured m_L/m_s ratio is 63% larger. We thus experimentally verified that the presence of the layer under a magnetic iron film can affect the EMCD signal of iron and, more importantly, the extracted m_L/m_s ratio of Fe 3d moments, in a way that a larger underlayer thickness may result in higher valuation of the m_L/m_s ratio. Our work provides important reference information for the potential application of the EMCD technique to composite nanomaterial systems.

See the supplementary material for the schematic diagram of the EMCD experimental setups, the magnetic hysteresis loops of our Fe/MgO(001) sample, and the elemental map at its interface.

This work was supported by the National Natural Science Foundation of China (Grant No. 51701031); the State Key Research and Development Program of MOST, China (Grant No. 2016YFB0700400); and China Postdoctoral Science Foundation (Grant No. 2018M631060). We thank S. Löffler for providing the simulation program.

Published under license by AIP Publishing

REFERENCES

[1]P. Schattschneider, S. Rubino, C. Hébert, J. Rusz, J. Kuneš, P. Novák, E. Carlino, M. Fabrizioli, G. Panaccione, and G. Rossi, Nature **441**, 486–488 (2006).
[2]D. Song, Z. Wang, and J. Zhu, Ultramicroscopy **201**, 1–17 (2019).
[3]L. Calmels, F. Houdellier, B. Warot-Fonrose, C. Gatel, M. J. Hÿtch, V. Serin, E. Snoeck, and P. Schattschneider, Phys. Rev. B **76**, 060409 (2007).
[4]B. Warot-Fonrose, F. Houdellier, M. J. Hÿtch, L. Calmels, V. Serin, and E. Snoeck, Ultramicroscopy **108**, 393–398 (2008).
[5]B. Warot-Fonrose, C. Gatel, L. Calmels, V. Serin, and P. Schattschneider, Ultramicroscopy **110**, 1033–1037 (2010).
[6]H. Ali, T. Warnatz, L. Xie, B. Hjörvarsson, and K. Leifer, Ultramicroscopy **196**, 192–196 (2019).
[7]Z. Wang, A. H. Tavabi, L. Jin, J. Rusz, D. Tyutyunnikov, H. Jiang, Y. Moritomo, J. Mayer, R. E. Dunin-Borkowski, Y. Rong, and J. Zhu, Nat. Mater. **17**, 221–225 (2018).
[8]S. Muto, J. Rusz, K. Tatsumi, R. Adam, S. Arai, V. Kocevski, P. M. Oppeneer, D. E. Bürgler, and C. M. Schneider, Nat. Commun. **5**, 3138 (2014).
[9]J. Rusz, S. Muto, J. Spiegelberg, R. Adam, K. Tatsumi, D. E. Bürgler, P. M. Oppeneer, and C. M. Schneider, Nat. Commun. **7**, 12672 (2016).
[10]X. Fu, B. Warot-Fonrose, R. Arras, G. Seine, D. Demaille, M. Eddrief, V. Etgens, and V. Serin, Phys. Rev. B **93**, 104410 (2016).
[11]Z. Q. Wang, X. Y. Zhong, R. Yu, Z. Y. Cheng, and J. Zhu, Nat. Commun. **4**, 1395 (2013).
[12]D. Song, G. Li, J. Cai, and J. Zhu, Sci. Rep. **6**, 18489 (2016).
[13]D. Song, J. Rusz, J. Cai, and J. Zhu, Ultramicroscopy **169**, 44–54 (2016).
[14]G. Li, D. Song, Z. P. Li, and J. Zhu, Appl. Phys. Lett **108**(24), 242414 (2016).
[15]D. Song, A. H. Tavabi, Z. A. Li, A. Kovács, J. Rusz, W. Huang, G. Richter, R. E. Dunin-Borkowski, and J. Zhu, Nat. Commun. **8**, 15348 (2017).
[16]C. Hébert, P. Schattschneider, S. Rubino, P. Novák, J. Rusz, and M. Stöger-Pollach, Ultramicroscopy **108**, 277–284 (2008).
[17]Z. C. Wang, X. Y. Zhong, L. Jin, X. F. Chen, Y. Moritomo, and J. Mayer, Ultramicroscopy **176**, 212–217 (2017).
[18]T. Thersleff, J. Rusz, B. Hjörvarsson, and K. Leifer, Phys. Rev. B **94**, 134430 (2016).
[19]X. Fu, B. Warot-Fonrose, R. Arras, K. Dumesnil, and V. Serin, Phys. Rev. B **94**, 140416 (2016).
[20]S. Löffler and P. Schattschneider, Ultramicroscopy **110**, 831–835 (2010).
[21]Z. S. Basinski, W. Hume-Rothery, and A. L. Sutton, Proc. R. Soc. London, Ser. A **229**(1179), 459–467 (1955).
[22]H. Bialas and K. Heneka, Vacuum **45**(1), 79–87 (1994).
[23]R. F. Egerton, *Electron Energy-Loss Spectroscopy in the Electron Microscope*, 3rd ed. (Springer, Berlin, 2011).
[24]J. Rusz, H. Lidbaum, S. Rubino, B. Hjörvarsson, P. M. Oppeneer, O. Eriksson, and K. Leifer, Phys. Rev. B **83**, 132402 (2011).

Published under license by AIP Publishing